Original Article

PROGRESS in MEDICAL PHYSICS 27(4), Dec. 2016
https://doi.org/10.14316/pmp.2016.27.4.203
pISSN 2508-4445, eISSN 2508-4453

Evaluating Correlation between Geometrical Relationship and Dose Difference Caused by Respiratory Motion Using Statistical Analysis

Dong-Seok Shin*, Seong-Hee Kang*, Dong-Su Kim*, Tae-Ho Kim*, Kyeong-Hyeon Kim*, Min-Seok Cho†, Yu-Yoon Noh*, Do-Kun Yoon*, Tae Suk Suh*

*Department of Biomedical Engineering, Research Institute of Biomedical Engineering, College of Medicine, The Catholic University of Korea,
†Department of Radiation Oncology, Asan Medical Center, Seoul, Korea

Dose differences between three-dimensional (3D) and four-dimensional (4D) doses could be varied according to the geometrical relationship between a planning target volume (PTV) and an organ at risk (OAR). The purpose of this study is to evaluate the correlation between the overlap volume histogram (OVH), which quantitatively shows the geometrical relationship between the PTV and OAR, and the dose differences. 4D computed tomography (4DCT) images were acquired for 10 liver cancer patients. Internal target volume-based treatment planning was performed. A 3D dose was calculated on a reference phase (end-exhalation). A 4D dose was accumulated using deformation vector fields between the reference and other phase images of 4DCT from deformable image registration, and dose differences between the 3D and 4D doses were calculated. An OVH between the PTV and selected OAR (duodenum) was calculated and quantified on the basis of specific overlap volumes that corresponded to 10%, 20%, 30%, 40%, and 50% of the OAR volume overlapped with the expanded PTV. Statistical analysis was performed to verify the correlation with the OVH and dose difference for the OAR. The minimum mean dose difference was 0.50 Gy from case 3, and the maximum mean dose difference was 4.96 Gy from case 2. The calculated range of the correlation coefficients between the OVH and dose difference was from -0.720 to -0.712, and the R-square range for regression analysis was from 0.506 to 0.518 (p-value <0.05). However, when the 10% overlap volume was applied in the six cases that had OVH value ≤ 2, the average percent mean dose differences were 34.80±12.42%. Cases with quantified OVH values of 2 or more had mean dose differences of 29.16±11.36%. In conclusion, no significant statistical correlation was found between the OVH and dose differences. However, it was confirmed that a higher difference between the 3D and 4D doses could occur in cases that have smaller OVH value.

Key Words: 4D dose, Overlap volume histogram, Respiratory motion, Geometrical relationship

Introduction

Intensity-modulated radiation therapy (IMRT) allowed delivering precise dose of radiation to tumors while minimizing damage of normal tissue and organ at risk (OAR). However, such a therapy is difficult to achieve for radiation therapy due to the presence of unintended movements such as peristalsis, cardiac impulse, and respiration. Particularly, the abdomen is a part of the human body that is influenced greatly by respiratory motions. Hence, a dose lower than the prescribed dose can be delivered to the tumor or a dose higher than the tolerance dose can be delivered to a normal tissue if the effect of the respiratory motion is not considered for the radiation therapy for liver cancer.

Owing to the recent commercialization of four-dimensional computed tomography (4DCT), information on movement and changes in tumors and OARs that result from respiration mo-

Received 10 November 2016, Revised 19 December 2016, Accepted 20 December 2016
Correspondence: Tae Suk Suh (suhsanta@catholic.ac.kr)
Tel: 82-2, Fax: 82-2-2258-7506

tion can be obtained from the respiratory phase of the patient from information in the image sets of three-dimensional computed tomography (3DCT).[1,2] The information on the movement of internal organs provided by the 4DCT can be used to plan radiation therapy using patient-specific internal target volume (ITV).[3,7,20] Furthermore, 4DCT also made four-dimensional (4D) radiation therapies such as breath-holding radiation therapy[6,19] or respiratory-gated radiation therapy[4,5] possible. Among them, ITV-based radiation therapy is a method that considers the coverage of tumor movements caused by respiratory motion and, consequently, includes a large margin in the planning target volume (PTV); it has been mainly used for clinical purposes. However, owing to the large margin included in the PTVs, there is a high possibility of a normal tissue or an OAR being exposed to radiation compared to other 4D radiation therapies.[3] Moreover, owing to the characteristics of the ITV-based radiation therapy, which focuses on the movement coverage of a tumor, there is a possibility of discrepancy between the actual delivery dose and the plan dose calculated using a dose prediction model when planning radiation therapy for an OAR near a PTV. One of the reasons for such a discrepancy is the change in the geometrical relationship between the PTV and the OAR because the tumor and the surrounding OARs move due to the respiratory motion. However, it is difficult to consider the discrepancies in doses that occur in ITV-based radiation therapy planning. One of the reasons for this is that even though the movement coverage is considered in the ITV, the dose calculated by the dose prediction model is based on one image from one phase—the reference phase—out of the many images of many phases from 4DCT.

Recently, various studies on 4D doses that reflect the effects of respiratory motion have attempted to address this problem.[9-13] Generally, a 4D dose is obtained by applying deformation vector fields (DVFs) obtained from deformable image registration (DIR) between a reference image and images from nine phases to each dose distribution calculated based on 10 phase images obtained from 4DCT. Hence, every dose distribution calculated from each phase image is considered and allows for estimating the actual delivered dose more accurately than the 3D dose, which is calculated from a single-phase image.

The difference between 3D and 4D doses is greatest near a PTV due to the motion of the tumor.[12] In this case, the difference between the predicted dose and the actual delivery dose of an OAR near a PTV can be significant. This may cause unexpected side effects after the therapy. Therefore, an accurate prediction of the dose to be delivered is required by calculating the 4D dose if major OARs are close to the tumor. However, 4D doses take more time to calculate compared to 3D doses, and hence, the related workload is heavy. Thus, clinical applications are limited. In order to address this problem, it is necessary to calculate 4D doses that can closely estimate real delivery doses by selecting patients with a high possibility of large differences in the 3D and 4D doses; in other words, patients with large dose differences at OARs near a PTV.[14] Consequently, time and labor spent on 4D dose calculations can be minimized and more accurate delivery doses can be estimated from 4D dose calculations when planning radiation therapies for selected patients. To achieve this, a method of selecting subjects and, consequently, a quantitative evaluation of the factors affecting the difference between 3D and 4D doses were required. Previous researches reported that factors such as size and movement of tumors can influence the differences in doses.[11,12] This research focused on one particular reason out of the many reasons cited for the difference in doses—the geometrical relationship changes between the PTVs and OARs caused by respiratory motion. Furthermore, this research assumed the geometrical relationship between the PTVs and OARs as a new factor. A quantitative definition of the geometrical relationship between the PTVs and OARs was reported using an overlap volume histogram (OVH) by Kazhdan et al.[15] In addition, Wu et. al. suggested that an OVH defining the geometrical relationship can help effectively manage the quality control of the IMRT planning for head-and-neck cancer patients,[16] and some research groups conducted researches on applying OVHs to radiation therapy.[8,18,21-24]

Therefore, this research used OVHs to define the geometrical relationship between the PTVs and OARs, such as relative location, distance, and shapes, quantitatively for cases with liver cancer patients that need to consider respiratory motion. This quantitative definition was used to select a new factor that caused differences between 3D and 4D doses. Furthermore, the correlation between the OVH and the difference between the 3D and 4D doses for an OAR near a PTV was analyzed statistically. As a result, the research was ex-

pected to contribute in suggesting a method for selecting subjects that needed 4D dose calculations and in allowing 4D doses for clinical applications.

Materials and Methods

1. Patient characteristics and imaging

This research was conducted based on information from 10 liver cancer patients; 5 patients had received three-dimensional conformal radiation therapy (3DCRT), and 5 patients had received stereotactic body radiotherapy (SBRT) between June 2014 to June 2015. Table 1 shows the therapy plan, PTV size, and center-of-mass (COM) distance between a PTV and the duodenum, which is the OAR, and the prescription dose for each case. For every patient's case, a CT scanner (SOMATOM Definition AS, Siemens Healthcare, Erlangen, Germany) and an ANZAI belt (Anzai Medical Company, Tokyo, Japan) were used to obtain 4DCT images at free-breathing state. The 4DCT images were sorted into 10 phase images using phase-based sorting, and the voxel size was 0.97 mm×0.97 mm×3.00 mm (coronal×sagittal×axial).

2. Delineation and dose calculations

The radiation therapy plan was conducted with end-exhalation phase in 4DCT as the reference image, and the therapy plan and

Table 1. Therapy plan and characteristics of each case. The center-of-mass (COM) distance is the distance from the planning target volume (PTV) to the organ at risk (OAR), which is the duodenum.

Case No.	Plan	PTV volume (cm^3)	COM distance (cm)	Prescription dose (Gy)
1	SBRT	83.37	7.35	40
2	SBRT	53.63	3.89	40
3	SBRT	54.59	5.43	40
4	SBRT	141.07	5.04	30
5	3DCRT	267.34	5.71	40
6	3DCRT	74.71	6.90	40
7	3DCRT	71.71	5.07	40
8	3DCRT	78.74	9.25	40
9	SBRT	36.30	2.97	30
10	3DCRT	67.20	4.34	40

SBRT: stereotactic body radiation therapy, 3DCRT: three-dimensional conformal radiation therapy.

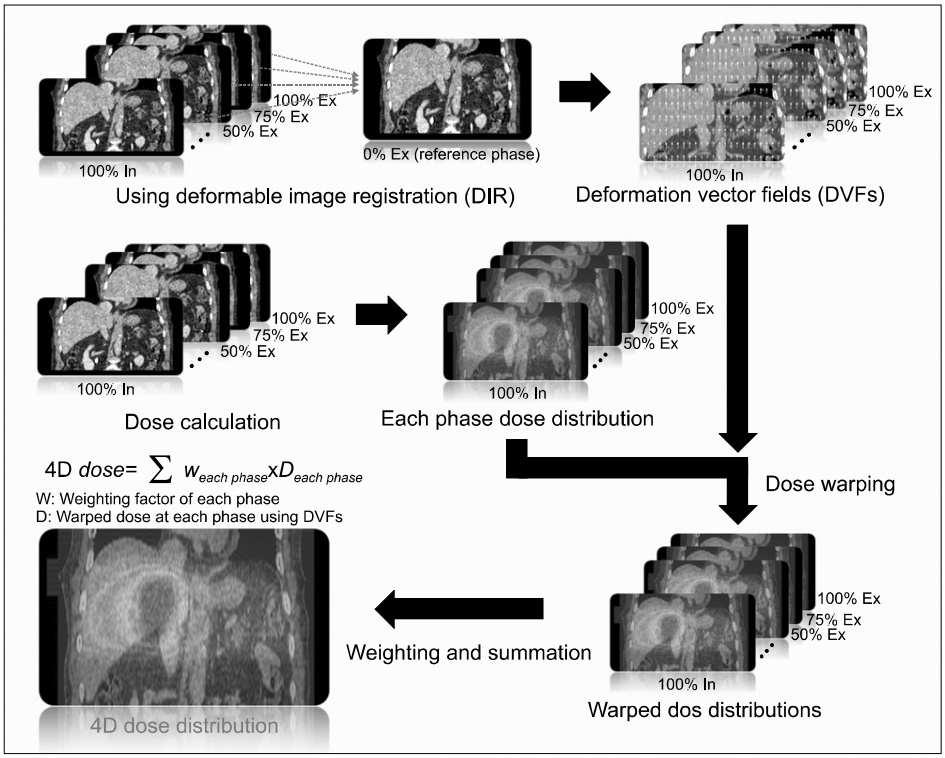

Fig. 1. Ssimple calculation process for four-dimensional doses (4D doses). First, deformable image registration was used to calculate the deformation vector fields (DVFs) for each phase image based on the end-exhalation phase image from four-dimensional computed tomography (4DCT). Second, the calculated DVFs were applied to each dose distribution that was calculated from each phase image to obtain the warped dose distributions. Finally, the warped dose distributions were weighted and summed up to calculate the 4D doses.

prescription dose for each case is shown in Table 1. From the reference image, the duodenum, which was the OAR near the PTV, was delineated. A gross target volume (GTV) was selected for each phase image. Integration of all the GTVs selected for each phase provided the ITV, and the PTV was defined by adding a 5-mm set-up margin to the obtained ITV. In addition, the duodenum was selected as the OAR based on the end-exhalation phase image. The collapsed cone convolution dose calculation algorithm of the therapy planning device (Pinnacle v8.0, Philips Medical System, Cleveland, OH) was used to calculate the dose distribution for each of the 10 phase images, which included the 3D dose in the existing phase image.

In order to run DIR, which was needed for calculating 4D doses, DIRART[17] was used through MATLAB 2010a (Math Works Inc., Natick, MA). By using the Horn and Schunck optical flow algorithm of DIR, DVFs between the end-exhalation phase image, reference image, and other nine phase images were obtained. The DVFs obtained from each phase were applied to the dose distributions calculated from each phase image to obtain dose distributions warped according to the reference phase image. Since this study obtained 4DCT images by phase-based sorting, same weighting (1/total number of 4DCT phase bin) was put on all 10 dose distributions—one 3D dose and 9 warped dose distributions—and were summed up to calculate the 4D doses. Fig. 1 shows the overall process of this 4D dose calculation. The difference between the 3D and 4D doses for the duodenum was calculated.

3. Overlap volume histogram

OVH is a two-dimensional (2D) curve that simultaneously expresses the geometrical relationship between a PTV and an OAR such as relative location, distance, and shape. When a uniform, arbitrary margin was applied to a PTV, it showed the ratio of the volume overlapping with the OAR in the OAR

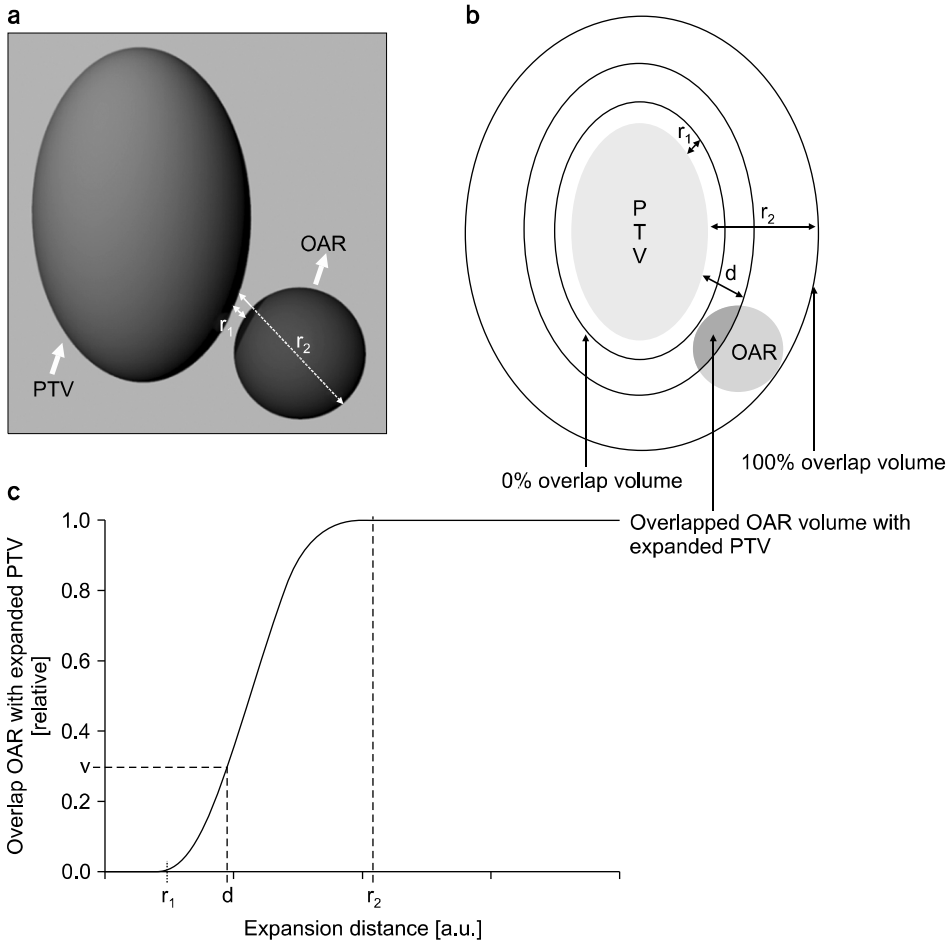

Fig. 2. Example of an overlap volume histogram (OVH). (a) three-dimensional view showing the geometrical relationship between the planning target volume (PTV) and the organ at risk (OAR), (b) two-dimensional view on the given PTV and OAR: r_1 is the maximum expansion distance where the expanded PTV and OAR did not overlap when PTV was expanded by an arbitrary margin. r_2 is the minimum expansion distance where the OAR was perfectly overlapped by the PTV expanded by an arbitrary margin. d is the margin size when the ratio of the overlapped volume (red area) between the expanded PTV and OAR to the volume of OAR was v, (c) OVH of given PTV and OAR.

volume.[15] Fig. 2(a) shows the geometrical relationship between the arbitrary PTV and the OAR in a 3D view, and Fig. 2(b) expresses Fig. 2(a) in a 2D view. Fig. 2(c) expresses this geometrical relationship between the PTV and OAR using an OVH. The horizontal axis displays the margin applied to the PTV, and, in this study, the size of such a margin is expressed as the expansion distance. The vertical axis displays the ratio of the volume overlapped between the OAR and PTV, which was expanded by a margin and the OAR volume. For example, v in Fig. 2(c) represents the ratio of the OAR volume to the overlapped volume (red area) between the OAR and the expanded PTV volume when the volume of the PTV was increased uniformly by an arbitrary expansion distance d in Fig. 2(b). In order to express the geometrical relationship between the PTV and OAR quantitatively using an OVH that was mentioned above, this study set a standard for the ratio of the volume overlapped between the expanded PTV and OAR to the volume of OAR as 10%, 20%, 30%, 40%, and 50%. For convenience, in this study, such standards are expressed as OVH_{10}, OVH_{20}, OVH_{30}, OVH_{40}, and OVH_{50}. The expansion distances were obtained for all patient cases based on the end-exhalation phase images obtained from 4DCT for each standard.

4. Statistical analysis

In order to evaluate the correlation between the 3D and 4D doses for the OVH and OAR, correlation analysis and regression analysis were conducted. Furthermore, the correlations between the COM distances between PTVs and OARs, the OVH, which was quantified using the standards for overlapping volume, and the dose differences between the 3D and 4D doses were statistically evaluated using regression analysis.

Results

1. Overlap volume histogram

Fig. 3 shows the OVH curves calculated from the 10 cases

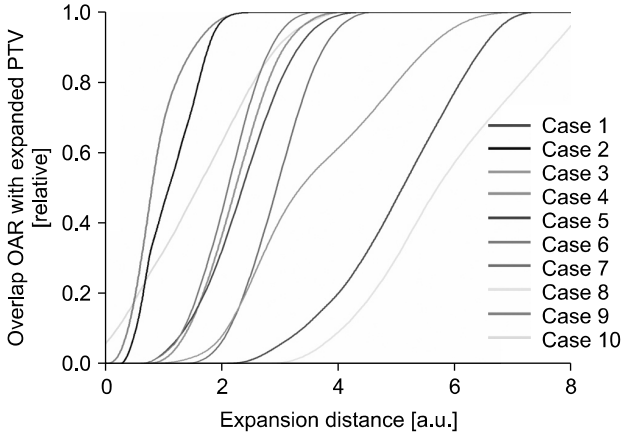

Fig. 3. Overlap volume histogram (OVH) for each case. The expansion distance of the horizontal axis represents the size of the margin used when the planning target volume (PTV) was expanded by an arbitrary margin. The vertical axis represents the ratio of the overlapped volume between the organ at risk (OAR) and expanded PTV, which was expanded by an arbitrary margin, to the volume of OAR.

Table 2. Expansion distance of each case according to the ratio of the overlapped volume between the organ at risk (OAR) and the planning target volume (PTV), which was expanded by an arbitrary margin to the OAR volume.

Case No.	Expansion Distance (a.u.)				
	OVH_{10}	OVH_{20}	OVH_{30}	OVH_{40}	OVH_{50}
1	3.38	4.01	4.43	4.79	5.10
2	0.54	1.66	0.76	0.92	1.11
3	2.13	2.42	2.69	2.95	3.34
4	1.42	1.67	1.88	2.08	2.25
5	1.34	1.68	1.95	2.16	2.36
6	1.33	1.59	1.78	1.95	2.11
7	2.10	2.36	2.59	2.76	2.94
8	4.05	4.52	4.99	5.34	5.71
9	0.41	0.54	0.63	0.72	0.80
10	0.20	0.58	0.93	1.27	1.59

OVH_x: Standard where the ratio between the overlapped volume of expanded PTV and the OAR to OAR volume is x%.

and most OVH curves had a similar shape except for case 3. Table 2 shows the expansion distance for each case according to the standards that quantified OVH (OVH_{10}, OVH_{20}, OVH_{30}, OVH_{40}, and OVH_{50}) in this study. The COM distance between the OAR and PTV was 9.25 cm, and case 8, where the PTV and OAR were separated by the greatest distance (Table 1), had the largest OVH value for every standard. However, for case 9, which had the smallest COM distance between the PTV and OAR at 2.97 cm (Table 1), the minimum expansion distance was not obtainable for standard OVH_{10}.

2. Dose differences between 3D and 4D doses

Table 3 shows the 3D mean dose, 4D mean dose, and the difference between the two values calculated for each case for the OAR (duodenum). A minimum mean dose difference value of 0.50 Gy was obtained in case 3, and a maximum mean dose difference of 4.96 Gy was obtained in case 2. A mean dose difference of more than 2.5 Gy between 3D and 4D doses was observed in the six cases.

Table 3. Mean three-dimensional dose (3D dose), mean four-dimensional dose (4D dose) and mean dose difference calculated for the duodenum, which was the organ at risk (OAR) for each case.

Case No.	$3D_{mean}$ (Gy)	$4D_{mean}$ (Gy)	Mean dose difference (Gy)
1	12.74	11.04	1.70
2	12.79	7.83	4.96
3	1.64	1.14	0.50
4	7.21	3.80	3.41
5	14.09	11.15	2.94
6	7.57	3.76	3.81
7	5.16	3.48	1.68
8	2.31	1.38	0.93
9	9.87	7.31	2.56
10	12.83	9.55	3.28

$3D_{mean}$: mean dose for 3D dose, $4D_{mean}$: mean dose for 4D dose.

3. Statistical analysis

Table 4 shows the regression analysis results for the expansion distance according to each OVH quantifying standard and the COM distance between the PTV and OAR. The coefficient of determination (R^2) was largest at 0.792 for the OVH_{40} standard, and the coefficient of determination (R^2) was smallest at 0.763 for the OVH_{10} standard. However, the standard error and the 95% confidence interval for the regression coefficient were found to have the minimum values when the standard was set to OVH_{50}. Fig. 4 shows the regression line and the scatter diagram for the regression analysis between the OVH_{50} standard, which had the smallest standard error, and the COM distance.

Table 5 represents the results for the correlation analysis and regression analysis between the mean dose differences of 3D and 4D doses and the expansion distance according to each OVH quantifying standard. For the case of the expansion distance of the quantified OVH, it was found that the correlation coefficient values changed from −0.720 to −0.712 as the standards changed, and the largest absolute value ($p\text{-value} < 0.05$) was observed for the OVH_{50} standard However, for the COM distance, the correlation coefficient value was 0.460, which was smaller than the value for the OVH. The coefficient of determination (R^2) for the regression analysis be-

Table 4. Regression analysis results of the quantified overlap volume histogram (OVH) and the center-of-mass (COM) distance between the planning target volume (PTV) and the organ at risk (OAR).

	R^2	Regression coefficient	Standard error	p-value	95% Confidence interval	
					Lower	Upper
OVH_{10}-COM distance	0.763	1.296	0.250	0.001	0.693	1.845
OVH_{20}-COM distance	0.779	1.175	0.221	0.001	0.665	1.685
OVH_{30}-COM distance	0.789	1.102	0.201	0.001	0.638	1.566
OVH_{40}-COM distance	0.792	1.057	0.192	0.001	0.615	1.499
OVH_{50}-COM distance	0.786	1.009	0.186	0.001	0.580	1.438

OVH_x: Standard where the ratio of overlapped volume between expanded PTV and OAR to OAR volume is x%, Standard error: the error value for regression coefficient.

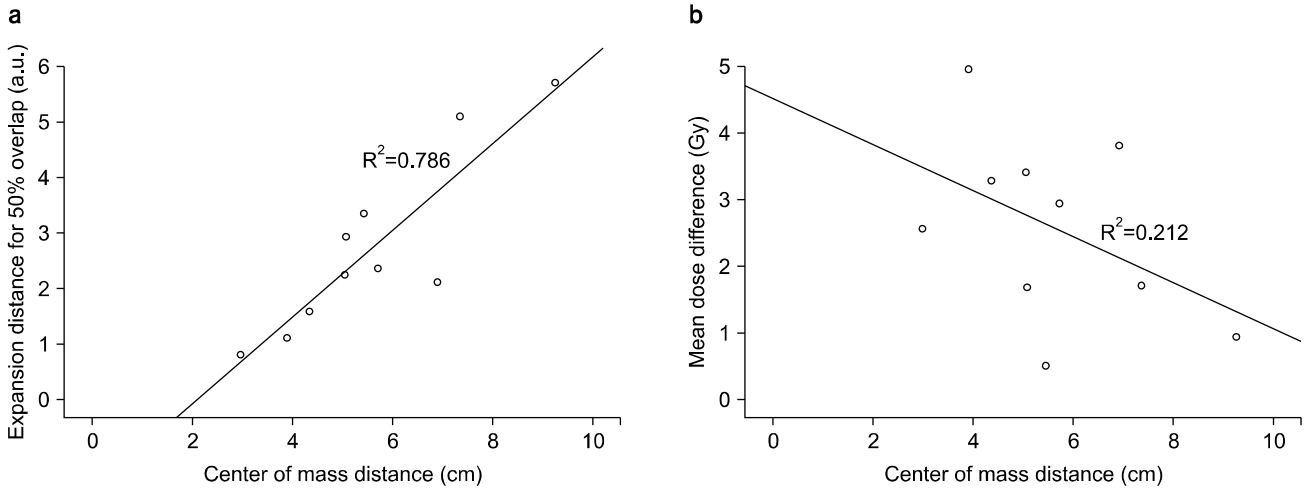

Fig. 4. Regression line and scatter diagram for the overlap volume histogram (OVH) and the center-of-mass (COM) distance between the planning target volume (PTV) and the organ at risk (OAR), and the mean dose differences between the four-dimensional dose (4D dose) and three-dimensional dose (3D dose) at the OAR. (a) Linear regression line and scatter diagram between the expansion distance and COM distance when the ratio of the OAR volume to the overlapped volume between the OAR and PTV expanded by an arbitrary margin was 50% (OVH_{50}), (b) Linear regression line and the scatter diagram between the mean dose difference and COM distance.

Table 5. Regression analysis results for the mean dose differences between three-dimensional doses (3D doses) and four-dimensional doses (4D doses), and the center-of-mass (COM) distance between the quantified overlap volume histogram (OVH), the organ at risk (OAR), and the planning target volume (PTV).

	Correlation coefficient R	R^2	Regression coefficient	Standard error	p-value	95% Confidence interval	
						Lower	Upper
OVH10-MDD	−0.717	0.514	−0.784	0.270	0.020	−1.407	−0.162
OVH20-MDD	−0.713	0.508	−0.715	0.249	0.021	−1.288	−0.142
OVH30-MDD	−0.715	0.511	−0.668	0.231	0.020	−1.201	−0.135
OVH40-MDD	−0.712	0.506	−0.637	0.222	0.021	−1.150	−0.124
OVH50-MDD	−0.720	0.518	−0.617	0.210	0.019	−1.103	−0.132
COM distance-MDD	0.460	0.212	−0.347	0.237	0.181	−0.892	0.198

OVH_x: Standard where the ratio of overlapped volume between expanded PTV and OAR to OAR volume is x%, MDD: mean dose difference, Standard error: the error value for regression coefficient.

tween the mean dose difference and OVH was calculated to be between 0.506 and 0.518. However, the coefficient of determination (R^2) between the mean dose difference and COM distance was calculated to be 0.212, and the p-value was found to be 0.181, which was greater than 0.05. Fig. 5 displays the scatter diagram and the linear regression line for the regression analysis between the expansion distance for each OVH quantifying standard and the mean dose difference between the 3D and 4D doses.

Discussion

Table 4 confirms that there was a significant statistical correlation between the COM distance from the PTV to the OAR and the OVH. One of the reasons for the abovementioned results was presumed to be the fact that the OVH was a factor that simultaneously represented the geometrical relationship between a PTV and an OAR, including the relative location, distance, and shapes. From the results in Table 5, it was confirmed that the OVH, which was a complex factor, had a

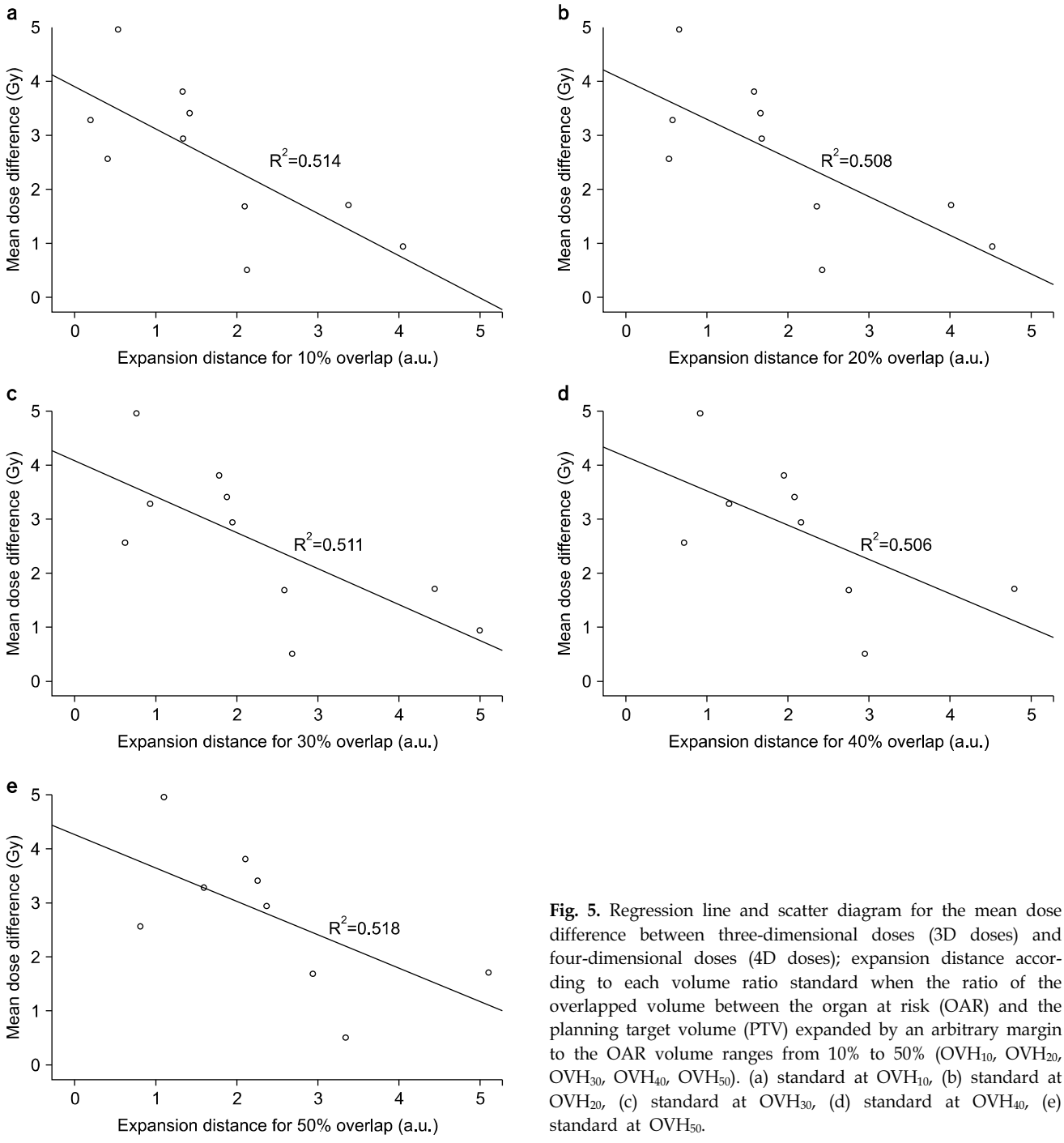

Fig. 5. Regression line and scatter diagram for the mean dose difference between three-dimensional doses (3D doses) and four-dimensional doses (4D doses); expansion distance according to each volume ratio standard when the ratio of the overlapped volume between the organ at risk (OAR) and the planning target volume (PTV) expanded by an arbitrary margin to the OAR volume ranges from 10% to 50% (OVH_{10}, OVH_{20}, OVH_{30}, OVH_{40}, OVH_{50}). (a) standard at OVH_{10}, (b) standard at OVH_{20}, (c) standard at OVH_{30}, (d) standard at OVH_{40}, (e) standard at OVH_{50}.

more significant statistical correlation with the differences between 3D and 4D doses as compared to the COM distance, which was a factor of singularity. However, since the OVH used in this study was expressed using a 2D curve, a standard, such as a specific overlapping ratio, was needed to express the OVH as a single quantitative number for each case. Since the standard for quantifying the OVH could influence the correlation of the differences between the 3D and 4D doses, this study set five arbitrary standards from 10% to 50% in 10% increments. Among these standards, OVH_{50}, when the ratio of

the overlapped volume between the expanded PTV and OAR and the volume of OAR was 50%, had the largest coefficient of determination (R^2) in the regression analysis. However, statistical results for all five quantified standards were similar. Such results were achieved because the slope of the curve for the OVH was similar for most the cases (Fig. 3). If the OVH curve was gradual, and, consequently, the change of expansion distances was large with changing OVH standards, it was predicted that the OVH standards would have a larger influence. However, although the OVH_{50} standard, which had the largest coefficient of determination (R^2) for the regression analysis, was applied in this study, there was no statistical significance between the geometrical relationship expressed with the OVH and the difference between the 3D and 4D doses. One of the reasons was because the geometrical relationship between the PTV and OAR established from a single standard phase image out of the many phase images obtained from 4DCT could not fully explain the differences between 3D and 4D doses that could have occurred from the geometrical changes in the PTV and OAR due to respiratory motion. In addition, the small number of cases made it difficult to obtain an accurate evaluation.

However, as shown in Fig. 5(a), the differences between 3D and 4D doses for the duodenum in the six cases that had an expansion distance of 2 or less under the OVH_{10} standard were 2.5 Gy or more, and the ratio of the mean dose difference was 34.80±12.42%. For four cases that had an expansion distance of 2 or more, the dose differences were 1.7 Gy or less, and the ratio for the mean dose difference was 29.16±11.36%. Furthermore, the mean dose differences for the 3D and 4D doses for the duodenum was reported to be large at 15.7±11.2% in the research by Jung et al. that studied 11 patient cases.[13] The results from this study were predicted to be from the geometrical relationship between the PTV and duodenum, and were significantly changing compared to the case with an opposite geometrical relationship due to the movements of the duodenum caused by the respiratory motion when the OVH expansion distance was small. That is, when the PTV and duodenum were in close proximity and their relative shapes were in a similar geometrical relationship. In other words, the duodenum had a possibility of the influence of the dose caused by a high dose gradient decreasing due to the geometrical relationship having a significant change from respiratory motion in the case where the OVH expansion distance was small. This could cause a large difference between the 3D and 4D doses. In addition, Table 3 shows that the 4D dose had a tendency of being smaller than the 3D dose for the duodenum, and this tendency was similar to the results obtained by Jung et al.[13] A study by Yeo et al.[12] also showed that 4D doses were either smaller or larger than 3D doses, depending on the types of OAR, including right and left kidneys, small bowel and others. Therefore, the tendency of 4D doses being smaller than 3D doses found in this study was considered to occur because of the indigenous locational characteristics of the OAR; in other words, the particular geometrical relationship between the PTV and OAR.

Among many OARs, including normal liver, kidney, duodenum, and stomach of a liver cancer patient, only the duodenum, which had the smallest volume, was selected as the OAR. This was because even though the PTV and OAR are in close proximity, the OAR with a relatively larger volume than the PTV causes the OVH curve to be relatively gradual since the vertical axis of OVH defines the volume ratio based on the volume of the OAR. As a result, the influence of the aforementioned OVH quantifying standards might increase, and the influence of the distance between the PTV and OAR might not be reflected in the OVH. Hence, the duodenum was selected as the OAR to minimize such influences. In future researches, additional analyses on various OARs based on several cases are required. Furthermore, the difference between the 3D and 4D doses would be predicted more accurately if the OAR movement data and the geometrical relationship between the PTVs and OARs are considered simultaneously.

Conclusion

This research assumed the geometrical relationship between a PTV and an OAR as a factor that influences the difference between 3D and 4D doses and statistically analyzed the correlation. Although the OVH, a factor that represents the geometrical relationship quantitatively, did not have a statistical significance with the dose differences as a single entity, it confirmed the possibility of obtaining larger dose differences for cases with small expansion distances that depend on the

OVH quantifying standards, compared to cases with contrary conditions. It was anticipated that if future researches use several clinical cases to simultaneously consider factors such as the scope of OAR movements and direction due to respiratory motion, and the geometrical relationship between the PTVs and OARs, assessing the correlation between these factors and the differences in the 3D and 4D doses at the OAR will be more accurate.

References

1. **Low DA, Nystrom M, Kalinin E, et al**: A method for the reconstruction of four-dimensional synchronized CT scans acquired during free breathing. Med Phys 30(6):1254-1263 (2003)
2. **Pan T, Lee T-Y, Rietzel E, Chen GTY**: 4D-CT imaging of a volume influenced by respiratory motion on multi-slice CT. Med Phys 31(2):333-340 (2004)
3. **Keall P**: 4-dimensional computed tomography imaging and treatment planning. Semin Radiat Oncol. 14(1):81-90 (2004)
4. **Ohara K, Okumura T, Akisada M, et al**: Irradiation synchronized with respiration gate. Int J Radiat Oncol Biol Phys 17(4):853-857 (1989)
5. **Hideo DK, Bruce CH**: Respiration gated radiotherapy treatment: a technical study. Phys Med Biol 41(1):83 (1996)
6. **Hanley J, Debois MM, Mah D, et al**: Deep inspiration breath-hold technique for lung tumors: the potential value of target immobilization and reduced lung density in dose escalation. Int J Radiat Oncol Biol Phys 45(3):603-611 (1999)
7. **Underberg RWM, Lagerwaard FJ, Cuijpers JP, Slotman BJ, van Sörnsen de Koste JR, Senan S al**: Four-dimensional CT scans for treatment planning in stereotactic radiotherapy for stage I lung cancer. Int J Radiat Oncol Biol Phys 60(4):1283-1290 (2004)
8. **Wu B, Pang D, Simari P, Taylor R, Sanguineti G, McNutt T**: Using overlap volume histogram and IMRT plan data to guide and automate VMAT planning: A head-and-neck case study. Med Phys 40(2):021714 (2013)
9. **Brock KK, McShan DL, Ten Haken RK, Hollister SJ, Dawson LA, Balter JM**: Inclusion of organ deformation in dose calculations. Med Phys 30(3):290-295 (2003)
10. **Starkschall G, Britton K, McAleer MF, et al**: Potential dosimetric benefits of four-dimensional radiation treatment planning. Int J Radiat Oncol Biol Phys 73(5):1560-1565 (2009)
11. **Valdes G, Robinson C, Lee P, et al**: Tumor control probability and the utility of 4D vs 3D dose calculations for stereotactic body radiotherapy for lung cancer. Med Dosim 40(1):64-69 (2015)
12. **Yeo UA, Taylor ML, Supple JR, et al**: Evaluation of dosimetric misrepresentations from 3D conventional planning of liver SBRT using 4D deformable dose integration. J Appl Clin Med Phys 15(6):188-203 (2014)
13. **Jung SH, Yoon SM, Park SH, et al**: Four-dimensional dose evaluation using deformable image registration in radiotherapy for liver cancer. Med Phys 40(1):011706 (2013)
14. **Starkschall G, Gibbons JP, Orton CG**: To ensure that target volumes are not underirradiated when respiratory motion may affect the dose distribution, 4D dose calculations should be performed. Med Phys 36(1):1-3 (2009)
15. **Kazhdan M, Simari P, McNutt T, et al**: A shape relationship descriptor for radiation therapy planning. Med Image Comput Comput Assist Interv 12(Pt 2):100-108 (2009)
16. **Wu B, Ricchetti F, Sanguineti G, et al**: Patient geometry-driven information retrieval for IMRT treatment plan quality control. Med Phys 36(12):5497-5505 (2009)
17. **Yang D, Brame S, El Naqa I, et al**: Technical Note: DIRART - A software suite for deformable image registration and adaptive radiotherapy research. Med Phys 38(1):67-77 (2011)
18. **Wang J, Jin X, Zhao K, et al**: Patient feature based dosimetric Pareto front prediction in esophageal cancer radiotherapy. Med Phys 42(2):1005-1011 (2015)
19. **Remouchamps VM, Vicini FA, Sharpe MB, Kestin LL, Marinez AA, Wong JW**: Significant reductions in heart and lung doses using deep inspiration breath hold with active breathing control and intensity-modulated radiation therapy for patients treated with locoregional breast irradiation. Int J Radiat Oncol Biol Phys 55(2):392-406 (2003)
20. **Liu HH, Balter P, Tutt T, et al**: Assessing Respiration-Induced Tumor Motion and Internal Target Volume Using Four-Dimensional Computed Tomography for Radiotherapy of Lung Cancer. Int J Radiat Oncol Biol Phys 68(2):531-540 (2007)
21. **Yang Y, Ford E.C, Wu B, et al**: An overlap-volume-histogram based method for rectal dose prediction and automated treatment planning in the external beam prostate radiotherapy following hydrogel injection. Med Phys 40(1):011709 (2013)
22. **Wu B, Ricchetti F, Sanguineti G, et al**: Data-driven approach to generating achievable dose-volume histogram objectives in intensity-modulated radiotherapy planning. Int J Radiat Oncol Biol Phys 79(4):1241-1247 (2011)
23. **Wu B, Pang D, Lei S, et al**: Improved robotic stereotactic body radiation therapy plan quality and planning efficacy for organ-confined prostate cancer utilizing overlap-volume histogram-driven planning methodology. Radiother Oncol 112(2): 221-226 (2014)
24. **Petit S.F, Wu B, Kazhdan M, et al**: Increased organ sparing using shape-based treatment plan optimization for intensity modulated radiation therapy of pancreatic adenocarcinoma. Radiother Oncol 102(1):38-44 (2012)